Computers, Materials & Continua
DOI: 10.32604/cmc.2023.031450
Article

Tech Science Press

Modeling and Analysis of UAV-Assisted Mobile Network with Imperfect Beam Alignment

Mohamed Amine Ouamri[1,2], Reem Alkanhel[3,*], Cedric Gueguen[1], Manal Abdullah Alohali[4] and Sherif S. M. Ghoneim[5]

[1]University of Rennes 1/ADOPNET team at IRISA laboratory, Rennes, 35000, France
[2]Faculté de Technologie, Laboratoire d'Informatique Médicale (LIMED), Université de Bejaia, Bejaia, 06000, Algérie
[3]Department of Information Technology, College of Computer and Information Sciences, Princess Nourah bint Abdulrahman University, P.O.Box 84428, Riyadh, 11671, Saudi Arabia
[4]Department of Information Systems, College of Computer and Information Sciences, Princess Nourah bint Abdulrahman University, P.O.Box 84428, Riyadh, 11671, Saudi Arabia
[5]Electrical engineering department, College of Engineering, Taif University P. O. Box 11099, Taif, 21944, Saudi Arabia
*Corresponding Author: Reem Alkanhel. Email: rialkanhal@pnu.edu.sa
Received: 18 April 2022; Accepted: 07 June 2022

Abstract: With the rapid development of emerging 5G and beyond (B5G), Unmanned Aerial Vehicles (UAVs) are increasingly important to improve the performance of dense cellular networks. As a conventional metric, coverage probability has been widely studied in communication systems due to the increasing density of users and complexity of the heterogeneous environment. In recent years, stochastic geometry has attracted more attention as a mathematical tool for modeling mobile network systems. In this paper, an analytical approach to the coverage probability analysis of UAV-assisted cellular networks with imperfect beam alignment has been proposed. An assumption was considered that all users are distributed according to Poisson Cluster Process (PCP) around base stations, in particular, Thomas Cluster Process (TCP). Using this model, the impact of beam alignment errors on the coverage probability was investigated. Initially, the Probability Density Function (PDF) of directional antenna gain between the user and its serving base station was obtained. Then, association probability with each tier was achieved. A tractable expression was derived for coverage probability in both Line-of-Sight (LoS) and Non-Line-of-Sight (NLoS) condition links. Numerical results demonstrated that at low UAVs altitude, beam alignment errors significantly degrade coverage performance. Moreover, for a small cluster size, alignment errors do not necessarily affect the coverage performance.

Keywords: Unmanned aerial vehicles; coverage analysis; stochastic geometry; millimeter wave; imperfect beam alignment

1 Introduction

Unmanned Aerial Vehicle (UAV) based-cellular network has recently attracted more attention due to its capacity to overcome some terrestrial network communication constraints [1,2]. For example, mmWave UAVs can easily establish line-of-sight (LoS) connections to ground users [3]. Additionally, UAV can assist terrestrial networks to prevent temporary congestion in ultra-dense places such as stadiums. In certain applications, UAVs can be used as a relay to improve energy efficiency in cellular networks. However, to maintain the high performance of UAVs based communication, the optimal UAVs deployment parameters are of fundamental importance [4]. Heterogeneity between UAV and ground base station requires an understanding of channel scenarios introduced such as the ground-to-ground (G2G) and air-to-ground (A2G) channels. Therefore, the modeling of these channels has received much attention in the literature [5,6]. To overcome spectral saturation, Millimeter Waves (mmWave) are largely considered one of the keys technology for the 5G network. Nevertheless, mmWave spectrum is susceptible to blockages and suffers from high propagation attenuation. To address the blocking effect, Beamforming can be applied to improve the signal quality and compensate for the additional path loss [7]. Currently, Stochastic Geometry is employed to study and analyze cellular network performance, in particular the deployment of base stations (BSs) and users' equipments (UEs) [8,9]. Indeed, BSs and UEs locations are modeled as Poisson Cluster Process (PCP) in several scenarios like sporting events. This distribution allows the coupling of UE and UAV locations, but also provides accurate models according to the 3rd Generation Partnership Project (3GPP).

1.1 Related Work

Several studies have recently addressed the performance analysis of UAV-assisted cellular networks, where different metrics were considered. For instance, authors in [10] analyzed downlink coverage and rate of a vertical heterogeneous network in both LOS and NLOS propagation. In this work, the authors assumed that the UAVs heights were fixed and their location distributed forms a Poisson Point Process (PPP). In [11], the authors investigated performance analysis for two scenarios: static UAVs and mobile UAVs. The proposed analytical framework adopts an appropriate (A2G) channel model that incorporated LoS and non-line-of-sight (NLoS) transmissions. However, beamforming has not been incorporated. In [12], stochastic geometry base PCP was proposed to model the UEs locations. Additionally, the impact of path loss exponent and UAV density on coverage probability was achieved. Moreover, PCPs were also introduced to the model device-to-device network in [13]. In this work, a special case of PCP namely the Matern cluster process (MCP) was used. The Cumulative Density Function (CDF) of distance distribution between UE and the adjacent/serving base station was derived. Authors in [14] proposed a unified spatial framework for UAV aided mmWave. More specifically, MCP and (TCP) were introduced to model and represent the BSs locations. A 3D blockage process and a 3D up tilted antenna model were introduced to characterize the impact of UAVs altitudes and positions. The signal-to-interference-plus-noise-ratio (SINR) coverage and outage probabilities were studied as the network performance metric in [15] and [16] respectively. First, in [15], the exact expression of coverage probability, which includes the effect of base stations (BSs) height, antenna pattern, and UAVs altitudes, was derived. Then, in [16], the outage probability and ergodic rate of Multi Input Multi Output (MIMO) were evaluated, when the transmit power of interference sources was proportional. Hou et al. [17] proposed a tractable approach to analyze coverage probability. The authors considered a scenario where the UAVs are placed between 3D obstacles. A more general study investigated the coverage optimization using stochastic geometry where the UEs were modeled as TCP [18]. This study aims to obtain an optimal UAVs height with maximum coverage probability. On the other extreme, in urban environments, it is necessary to keep

UAVs at low altitudes to reduce path loss. However, at this height, alignment errors are significant due to environmental obstacles such as large buildings and shadow zones.

1.2 Contributions

As discussed above, stochastic geometry is a promising power tool to provide autonomous and effective analysis for UAV-assisted wireless network performance. To address the coverage analysis challenges, considering the limitations of the existing models such as different heights of the drones, and beams alignment errors, The coverage probability while taking into account the two different challenges should be studied. First, although coverage analysis has been well studied in the literature, few articles have dealt with the problem when drones are positioned at different altitudes. In reality, drones cannot be positioned at identical heights depending on the propagation environment and building density. On the other hand, 5G wireless networks are very dense, requiring the involvement of robust technology to improve their coverage and capacity. Therefore, beamforming is applied in several UAV scenarios to enhance coverage, but there are still errors in the beam alignment, which degrades the association of users with their Base Station and as a result, poor coverage is experienced.

Motivated by these considerations, in this paper, a detailed performance analysis of a UAV-assisted cellular network over the Nakagami-m channel with Imperfect beam alignment was presented. The main contribution of this document can be summarized as follows:

- An analytical framework to analyze the coverage probability of UAV-assisted mobile networks under clustered users was suggested. Compared to [13], all UAV were located at different heights. Moreover, the system performance should be analyzed exactly when the UAVs were located at certain heights with imperfect beam alignment. Based on [19], an exact expression of coverage probability for typical UEs located at origin by adopting imperfect beam alignment was driven. The path loss model is different between aerial and ground tiers in both LoS and NLoS links.
- The proposed analysis provided several useful conclusions. First, it revealed that at low UAVs altitudes, beam alignment errors significantly degrade coverage performance. Second, our investigation showed that there was an optimal value for the imperfect beam alignment, which should not be exceeded to improve coverage probability

The remainder of this paper is organized as follows. In Section 2, the system and channel model was introduced. Section 3, association probability was derived. In Section 4, the exact expression of Coverage probability was obtained. In Section 5, some numerical results were presented to confirm the accuracy of the model. Finally, the conclusion and perspectives were presented in Section 6.

2 System Model

The system model illustrated in Fig. 1 was considered. The UAVs are deployed at different heights H_z according to the Homogeneous Poisson Point Process (HPPP) Φ_{UAV} with density $\lambda_{UAV} > 0$. Ground Bases Stations (GBSs) are spatially distributed according to HPPP Φ_{GBS} with density $\lambda_{GBS} > 0$. Each user was supposed to be clustered around the base station symmetrically independently and identically distributed according to a Gaussian distribution with zero mean and variance σ^2 [20]. Without any loss of generality, all BSs transmit at the same power transmission. Moreover, the thermal noise was negligible compared to the interferences. In this study, typical UE was associated with a single BS i.e., UAV or GBS, which provided the maximum received signal power. Tab. 1 defines all acronyms and notation used in this article.

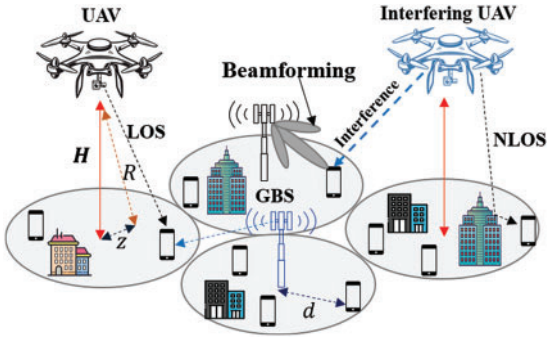

Figure 1: System model: UAV assisted cellular network in both LoS and NLoS link

Table 1: Table of notations

Notation	Explanation
$\lambda_{UAV}, \lambda_{GBS}$	Density of UAV and GBS.
σ^2	Gaussian distribution with zero mean and variance.
$P_{UAV}^{LOS}(r), P_{UAV}^{NLOS}(r)$	LoS/NLoS probabilities functions for UAV links.
$P_{GBS}^{LOS}(r), P_{GBS}^{NLOS}(r)$	LoS/NLoS probability function for GBS links.
$PL_{U}^{LOS}(r), PL_{U}^{NLOS}(r)$	Path loss for UAV.
$\alpha^{LOS}, \alpha^{NLOS}$	Path loss exponents for LoS and NLoS.
$\varphi^{LOS}, \varphi^{NLOS}$	Additional path loss for LoS and NLoS links.
A^{LOS}, A^{NLOS}	Path loss at a reference distance of $r = 1km$.
$f_h(x)$	Normalized Gamma distribution for channel Gain.
$\Gamma(m)$	Gamma function.
P_j, P_i	Power transmission for UAV and GBS respectively.
$\mathcal{A}_{UAV}^{k}, \mathcal{A}_{GBS}^{k}$	Association probabilities for UAV and GBS.
$\gamma_{UAV}, \gamma_{GBS}$	SINR fir UAV and GBS respectively.
$\mathcal{P}_{c,UAV}^{k}, \mathcal{P}_{C,GBS}^{k}$	Downlink coverage probabilities for UAV and GBS
$\mathcal{P}_{c,TOT}^{k}$	Total coverage probability of the network

2.1 Channel Model

To study the proposed model accurately, the LoS and NLoS links were examined separately, as well as their probabilities of occurrence. The LoS and alos NLoS probabilities depended on the environment propagation. Note that, for UAV-UE communication, the link probability was related to the UAV height. In urban scenarios, the effect of blockages was considerable. However, the probabilities functions of LoS/NLoS can be further given by [13].

For UAV-UE

$$P_{UAV}^{LOS}(r) = \frac{1}{1 + b\, exp\left(-c\left(\frac{180}{\pi} tan^{-1}\left(\frac{H_z}{r}\right) - b\right)\right)} \tag{1}$$

where b and c are constants that depend on the environment. The NLoS link probability is given by

$$P_{UAV}^{NLOS}(r) = 1 - P_{U}^{LOS}(r) \tag{2}$$

For GBS-UE

$$P_{GBS}^{LOS}(r) = e^{-\gamma r} \tag{3}$$

where γ is the blockage parameter.

2.2 Path Loss

In contrast to path loss model proposed in [11], our model incorporated different path loss for each tier (i.e., UAV and GBS). For the A2G link, the path loss model was formulated as follows

$$PL_{U}^{LOS}(r) = \varphi^{LOS}(r^2 + {H_z}^2)^{\frac{\alpha^{LOS}}{2}} \tag{4}$$

$$PL_{U}^{NLOS}(r) = \varphi^{NLOS}(r^2 + {H_z}^2)^{\frac{\alpha^{NLOS}}{2}} \tag{5}$$

where H_z is the altitude variation of the UAVs in meters, r is the distance between UE and the projection of UAV in the 2-D plane, φ^{LOS} and φ^{NLOS} are the additional path loss for LoS and NLoS links respectively. As in our previous work [21], the G2G propagation model is given by

$$PL_{S}^{k}(r) = \begin{cases} PL^{LOS}(r) = A^{LOS} r^{-\alpha^{LOS}} \\ PL^{NLOS}(r) = A^{NLOS} r^{-\alpha^{NLOS}} \end{cases} \tag{6}$$

where $PL^{LOS}(r)$ and $PL^{NLOS}(r)$ are the path loss functions for the LoS and NLoS transmission respectively. In addition, A^{LOS} and A^{NLOS} represent the path loss at a reference distance of $r = 1\ km$, α^{LOS} and α^{NLOS} are the LoS and NLoS path loss exponents.

2.3 Fading

Small-scale fading is a property of radio propagation caused by the existence of reflectors and scatterers. In fact, several versions of the transmitted signal reach the user, where each version was distorted in terms of amplitude, phase, and angle of arrival. In our model, Nakagami-m fading was used to model the fading channels with the shape parameter given by (N_{Los}, $1/N_{Los}$) and (N_{NLos}, $1/N_{NLos}$) for LoS and NLoS links, respectively [21]. Compared to Rayleigh fading, the Nakagami-m fading model gives a diversity order of m. Another reason, why was the Nakagami-m model suggested? His mathematical form is more analytically tractable to analyze in NLoS environment. Then, the channel gain $h_k$is normalized Gamma distribution given by [16].

$$f_h(x) = \frac{m^m}{\Gamma(m)} x^{m-1} e^{-mx} \quad x > 0 \tag{7}$$

where $\Gamma(m) = \int_0^\infty x^m e^{-x} dx$ is the Gamma function.

2.4 Imperfect Beam Alignment

To improve communication between the base station and user, directional beamforming [22] was used to focus a signal in a specific UE direction. However, UE and its serving base station adjusted the orientation of their antennas after estimating the angles of arrival (AoAs) and angles of departure (AoDs). The objective of this approach is to maximize directivity gain. Nevertheless, due to errors in the installation of antennas in practice, estimation errors in directivity angles could be made as shown

in Fig. 2. For the associated BS-UE pair, the imperfect beam alignment was modeled as a truncated Gaussian distributed variable [23] where the expression was given by

$$f_{\delta}(t) = \frac{\sqrt{\frac{2}{\pi\sigma^2}} e^{-\frac{t^2}{2\sigma^2}}}{erf\left(\frac{\pi}{\sqrt{2}\sigma}\right) - erf\left(-\frac{\pi}{\sqrt{2}\sigma}\right)}, t \in (-\pi, \pi] \tag{8}$$

where σ is the standard deviation and is usually applied to indicate the variability of beam alignment error. $erf\left(\frac{\pi}{\sqrt{2}\sigma}\right)$ is the error function computed as $erf\left(\frac{\pi}{\sqrt{2}\sigma}\right) = 2\int_0^{\frac{\pi}{\sqrt{2}\sigma}} e^{-t^2} dt/\sqrt{\pi}$.

$$\begin{cases} f_{m_R} = \dfrac{erf\left(\dfrac{\pi - 2cos^{-1}\left(\dfrac{1.391}{\pi\rho}\right)}{2\sqrt{2}\sigma_R}\right)}{\text{erf}\left(\dfrac{\pi}{\sqrt{2}\sigma_R}\right)} \\ f_{m_T} = \dfrac{erf\left(\dfrac{\pi - 2cos^{-1}\left(\dfrac{1.391}{\pi\rho}\right)}{2\sqrt{2}\sigma_T}\right)}{\text{erf}\left(\dfrac{\pi}{\sqrt{2}\sigma_T}\right)} \end{cases} \tag{9}$$

where σ_R, σ_T are beam alignment error standard deviations of the receiving (transmitting) antenna array. $\rho < 1/2$ is the number of antenna elements. To obtain the association probability of a typical UE with appropriate BS, it is necessary to know the distance distribution between UE and BSs in each tier. The UE is located at a distance D from the cluster center as illustrated in Fig. 3, the density function of the distance between UE and UAV for TCP is given by proposition 1.

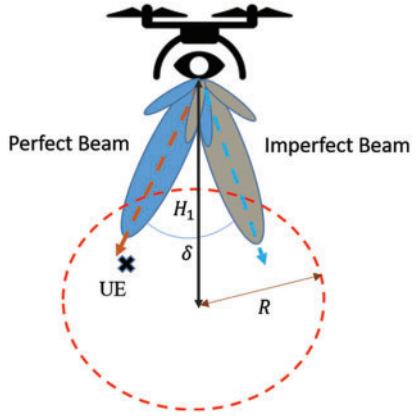

Figure 2: Imperfect beam alignment

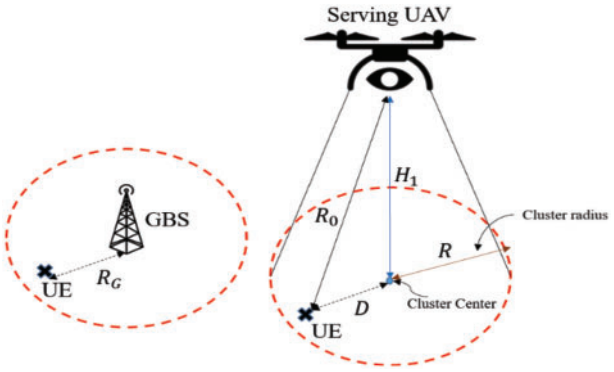

Figure 3: Distance separating the user from UAV and GBS

3 Users Association Approach

User association is an important step in a communication network and significantly affects network performance. It generally depends on the radio link, the distance between the user and BSs, and also the power transmission. Consequently, the user probability association is based on different schemes such as minimum load or maximum distance BS, and maximum received signal power. As mentioned above, in this work, we focus on the case where UE is connected with the BSs (UAV or GBS) that provides maximum received signal power and can be given mathematically as

$$P_j G_j PL_j(r)^{-1} \geq P_i G_i PL_i(r)^{-1} \quad \forall j \neq i, i \in \Phi_{GBS} j \in \Phi_{UAV} \tag{10}$$

where P_j, P_i is the power transmission, $G = m_R m_T$ is directional antenna gain and its probability distribution can be expressed by [19] as

Proposition 1: The PDF and CDF of the distance separated UE located at distance D from the cluster center to the nearest UAV can be expressed as:

$$\text{PDF}: f_{R_0}(r_0 | D, \sigma) = \frac{r_0}{\sigma^2} exp\left(\frac{D^2 - {r_0}^2}{2\sigma^2}\right) I_0\left(\frac{r_0 D}{\sigma^2}\right) \tag{11}$$

$$\text{CDF}: F_{R_0}(r_0 | D, \sigma) = 1 - Q_1\left(\frac{D}{\sigma}, \frac{r_0}{\sigma}\right) \tag{12}$$

where $Q_1\left(\frac{D}{\sigma}, \frac{r_0}{\sigma}\right) = \int_{\frac{r_0}{\sigma}}^{\infty} \frac{te^{-t^2+\left(\frac{D}{\sigma}\right)^2}}{2} I_0\left(\frac{D}{\sigma}t\right) dt$ is the Marcum Q-function. The proof follows the same steps as [24, Corollary 1]. In addition, the distance R_G separating a typical UE to the nearest LOS/NLOS GBS can be derived as

$$\text{PDF}: f_Y(R_G) = \frac{R_G}{\sigma^2} exp\left(-\frac{{R_G}^2}{2\sigma^2}\right) \tag{13}$$

$$\text{CDF}: F_Y(R_G) = exp\left(-\frac{{R_G}^2}{2\sigma^2}\right) \tag{14}$$

In the following Lemma, the probability that the UE was associated with a LOS/NLOS UAV or GBS. This can be evaluated by assuming that the number of drones per cluster was fixed and using

the ordered statistics of the distance distribution of the cluster BSs points to the typical user located at distance.

$$\mathcal{A}^{k}_{UAV} = 1 - \int_{0}^{\infty} \exp\left(-2\pi\lambda_{UAV}\int_{0}^{\sqrt{\omega}} tP^{k}_{UAV}(t)\right) f_{R_0}(r|D,\sigma)dr \tag{15}$$

$$\mathcal{A}^{k}_{GBS} = 1 - \int_{0}^{\infty} \exp\left(-2\pi\lambda_{GBS}\int_{0}^{\left(\frac{P_i G_i \varphi^k}{P_j G_j A^k}\left(r_j{}^2+H_z{}^2\right)^{\frac{\alpha^k}{2}}\right)^{\alpha^k}} tP^{k}_{GBS}(t)\right) f_Y(R_G)\,dr \tag{16}$$

4 Performance Analysis

This section presented the performance analysis of the proposed system with imperfect beam alignment. However, the metric that has been selected to be estimated was the coverage probability.

4.1 SINR Model

The analysis of this special case will provide important information about the network performance in more general contexts. Particularly, the coverage probability can be defined as the probability that signal-to-interference-plus-noise-ratio experienced by a typical user is greater than the desired threshold τ. Mathematically, the formula is $\mathcal{P}^{k}_{c,UAV} = \mathbb{P}[SINR_{UAV} > \tau]$ and $\mathcal{P}^{k}_{c,GBS} = \mathbb{P}[SINR_{GBS} > \tau]$. In our approach, the serving UAV was only interfered with by adjacent UAVs. On the other hand, the serving GBS was interfered with by both entities (UAV and SBS). According to this assumption, the SINR at typical UE can be expressed as

$$\gamma_{UAV} = \frac{P_{UAV}G_{UAV}h_{UAV}PL^{k}_{UAV}(r)^{-1}}{\sum_{UAV'\neq UAV}P_{UAV'}G_{UAV'}h_{UAV'}PL^{b}_{UAV'}(r)+\sigma^2} \tag{17}$$

$$\gamma_{GBS} = \frac{P_{GBS}G_{GBS}h_{GBS}PL^{k}_{GBS}(r)^{-1}}{\sum_{GBS'\neq GBS}P_{GBS'}G_{GBS'}h_{GBS'}PL^{b}_{GBS'}(r)+I_{UAV}+\sigma^2} \tag{18}$$

Lemma: The probability that a typical UE is associated with UAV/GBS in both LOS and NLOS conditions can be expressed by (15) and (16).

Proof: See Appendix A

where $I_{UAV} = \sum_{UAV\in\Phi_{UAV}} P_{UAV}G_{UAV}h_{UAV}PL^{k}_{UAV}(r)$ is the interference from adjacent UAV and σ^2 represent the variance of the additive white Gaussian noise component. The following theorem characterizes the coverage probability when the UE is served by UAV and GBS respectively. In this theorem, we also obtain the Laplace transform of different interference indicated above.

Theorem: For the special case of TCP, the downlink coverage probability for typical UE in both LOS/NLOS links can be expressed by

$$\mathcal{P}^{k}_{c,UAV} = \mathbb{E}_{G_{UAV}}\left[\sum_{n=1}^{N_k}(-1)^{n+1}\binom{N_k}{n}e^{-\mu\sigma^2}\mathcal{L}_{I_{UAV'}}(\mu)\right] \tag{19}$$

$$\mathcal{P}^{k}_{C,GBS} = \mathbb{E}_{G_{GBS}}\left[\sum_{n=1}^{N_k}(-1)^{n+1}\binom{N_k}{n}e^{-q\sigma^2}\mathcal{L}_{I_{UAV}}(\mu)\mathcal{L}_{I_{GBS'}}(\varepsilon)\right] \tag{20}$$

Proof: See Appendix B

4.2 Total Coverage Probability

In this subsection, after deriving the formulas for the association probabilities and conditional coverage probabilities, now the total coverage probability will be calculated. The overall network coverage in a UAV assisted mobile network was the sum of coverage offered by both tiers and can be expressed as

$$\mathcal{P}^{k}_{c,TOT} = \sum_{i=1}^{2} \mathcal{C}_i \tag{21}$$

where $\mathcal{C}_i = \mathcal{P}^{k}_{c,i}\mathcal{A}^{k}_{i}$. Therefor, by substituting (19), (20), (15) and (16) we obtain the expression for the total coverage probability as

$$\begin{aligned}\mathcal{P}^{k}_{c,TOT} = {} & \mathbb{E}_{G_{UAV}}\left[\sum_{n=1}^{N_k}(-1)^{n+1}\binom{N_k}{n}e^{-\mu\sigma^2}\mathcal{L}_{I_{UAV'}}(\mu)\right]\times 1 - \int_0^{\infty}\exp\left(-2\pi\lambda_{UAV}\int_0^{\sqrt{\omega}} tP^{k}_{UAV}(t)\right)\\ & \times f_{R_0}(r\,|D,\sigma)\,dr + \mathbb{E}_{G_{GBS}}\left[\sum_{n=1}^{N_k}(-1)^{n+1}\binom{N_k}{n}e^{-q\sigma^2}\mathcal{L}_{I_{UAV}}(\mu)\mathcal{L}_{I_{GBS'}}(\varepsilon)\right]\\ & - \int_0^{\infty}\exp\left(-2\pi\lambda_{GBS}\int_0^{\vartheta} tP^{k}_{GBS}(t)\right)\times f_Y(R_G)\,d\end{aligned} \tag{22}$$

where $\vartheta = \left(\frac{P_i G_i \varphi^k}{P_j G_j A^k}\left(r_j^2 + H_z^2\right)^{\frac{\alpha^k}{2}}\right)^{\alpha^k}$

5 Simulation Results

The analytical expression for the association probability and coverage probability has been derived in Sections 3 and 4, respectively. In this section, the coverage probability expression obtained was validated against Monte Carlo simulations using MATLAB. Results were based on the impact of UAV height and the imperfect beam alignment. The transmit power of SBS and UAV were 30 and 24 dBm, respectively. For our simulation, all necessary parametric values were given in Tab. 2.

Table 2: Simulation parameters

Parameters	Values
SBS and UAV density $\boldsymbol{\lambda_S}$, $\boldsymbol{\lambda_U}$	$10^{-2}/\mathrm{m}^2$ $10^{-3}/\mathrm{m}^2$
Carrier frequency $\boldsymbol{f}$	28 GHz
additional and exponent path loss $\boldsymbol{\alpha^{LOS}}$, $\boldsymbol{\alpha^{NLOS}}$, $\boldsymbol{\varphi^{LOS}}$, $\boldsymbol{\varphi^{NLOS}}$	2,3,1,1
SINR threshold $\boldsymbol{\tau}$	−90 dBm [13]
Noise power $\boldsymbol{\sigma^2}$	−174 dBm/Hz

Fig. 4 illustrated the impact of beam alignment errors on the coverage probability with different values of UAV height. It is observed that the beam alignment error increases the coverage probability deteriorates. Indeed, this degradation was considerable when the UAV height increased. The reason was that when the UAV height increased the misalignment occurred with a high probability. Moreover,

the distance between the drone and the UE became significant, which enhanced attenuation. As can be seen from Fig. 5, the coverage probability was significantly decreased when the cluster size was increased. This was mainly due to the increase in path loss (enhanced distance between UAVs and UE). It was clearly shown that for a small cluster size, alignment errors did not necessarily affect the coverage performance and the same results as when UE and BSs were perfectly aligned. This can be explained as when the cluster was reduced, the UE and its serving base station adjusted the orientation of their antennas easily over a large distance. In addition, despite the estimation errors of (AoAs) and (AoDs), when the radius of the cluster was small, the received power by the user was high, because they were closer to the base station and the losses become minimal. To validate the coverage analysis, the estimated results were plotted against drone density. It was obvious from the figure that the analytical results were reasonably consistent with the simulation results. Indeed, Fig. 6 illustrated the impact of UAV density at different values of alignment error.

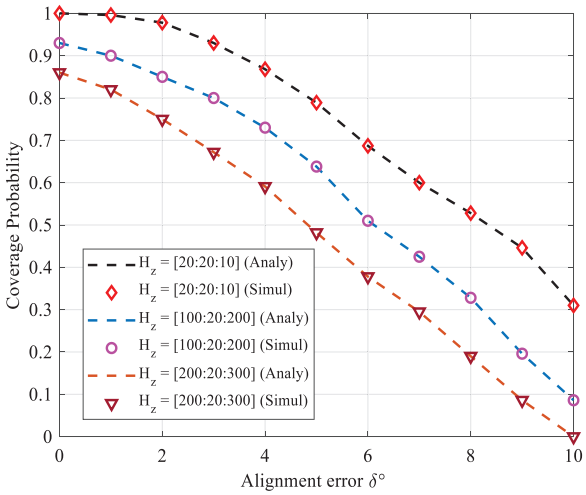

Figure 4: Coverage probability as a function of alignment error with different UAV height variation H_z

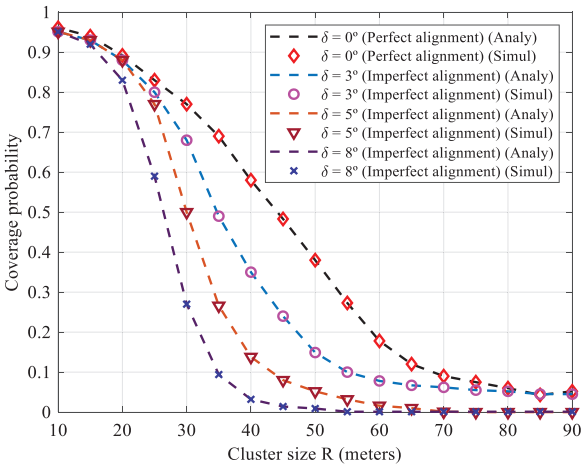

Figure 5: Coverage probability as function of cluster size with different imperfect alignment δ

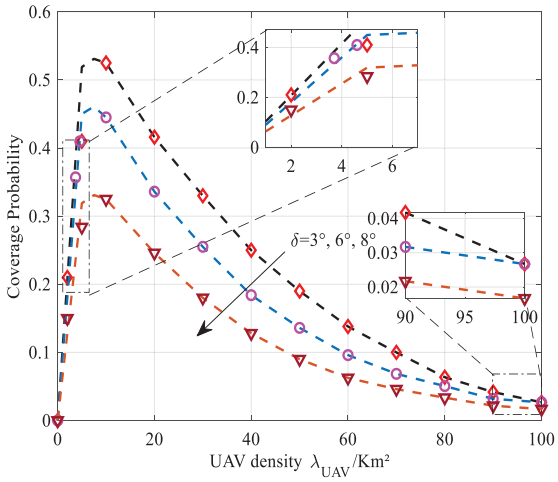

Figure 6: Coverage probability as function of UAV density λ_{UAV} with different imperfect beam alignment δ

It can be observed from the figure that when the UAV density increased slightly, the coverage probability was initially improved. The reason was that the distance between UE and UAV was reduced. Therefore, the probability of having a LOS link was high. Contrarily, increasing UAV density significantly led to higher interference. On the other hand, increasing UAV deployment results in increased beam alignment error. It was due to inadequate exploitation of beamforming gains, i.e., the base station and the user did not perfectly adjust their azimuth, main lobe, and side lobe for each entity. In Fig. 7, coverage probability as a function of SINR with different beam alignments was plotted. From this figure, the coverage performance of the derived analytical statement was sufficiently accurate to evaluate the coverage probability of the system. Indeed, as the SINR threshold increases the coverage probability decreases. It can also be seen that when the UE and its serving BS (UAV or GBS) were note aligned perfectly, the coverage probability was significantly reduced

.

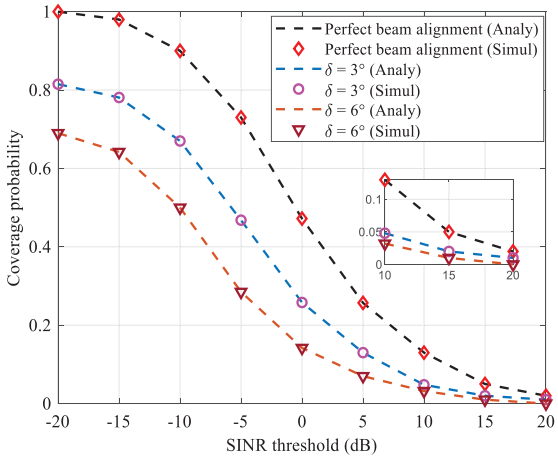

Figure 7: Coverage probability as a function of SINR threshold with perfect/imperfect beam alignment δ

6 Conclusion

In this paper, the downlink coverage analysis for UAV-assisted mobile networks with imperfect beam alignment has been investigated in both LOS and NLOS propagation. Our framework assumed that all UAVs were deployed at different heights. Specifically, stochastic geometry-based techniques were used to derive the exact expression of coverage probability, which can be affected by inter-cell interference. First, the association probability and distance distribution were obtained in the case of the Thomas cluster process. Then, based on the proposed model the coverage probability was derived and evaluated by integrating the impact of the beam alignment error. Using numerical results, it was shown that at low UAVs altitude, beam alignment errors significantly degraded coverage performance. Moreover, alignment errors did not affect the coverage probability at a small cluster size. There were many interesting questions to be addressed in the future, and some of them are listed below:

- Coverage and rate for UAV-assisted small cells by introducing inter-cell interference coordination between UAVs were analyzed.
- Analyze the performance when the UAVs are equipped with an antenna array and use the 3D beamforming model.
- Study the performance of UAVs swarm in 3D blocking environments with cooperation methods.

Acknowledgement: The authors express their gratitude to Princess Nourah bint Abdulrahman University Researchers Supporting Project number (PNURSP2022R323), Princess Nourah bint Abdulrahman University, Riyadh, Saudi Arabia, and Taif University Researchers Supporting Project Number TURSP-2020/34, Taif, Saudi Arabia.

Funding Statement: This work was supported by Princess Nourah bint Abdulrahman University Researchers Supporting Project number (PNURSP2022R323), Princess Nourah bint Abdulrahman University, Riyadh, Saudi Arabia, and Taif University Researchers Supporting Project Number TURSP-2020/34, Taif, Saudi Arabia.

Conflicts of Interest: The authors declare that they have no conflicts of interest to report regarding the present study.

References

[1] W. Huang, J. Peng and H. Zhang, "User-centric intelligent UAV swarm etworks: Performance analysis and de-sign insight," *IEEE Access*, vol. 7, pp. 181469–181478, 2021.

[2] O. Sami Oubbati, M. Atiquzzaman, T. Ahamed Ahanger and A. Ibrahim, "Softwarization of UAV networks: A survey of applications and future trends," *IEEE Access*, vol. 8, pp. 98073–98125, 2020.

[3] M. Lahmeri, M. A. Kishk and M. Alouini, "Stochastic geometry-based analysis of airborne base stations with laser-powered UAVs," *IEEE Communications Letters*, vol. 24, no. 1, pp. 173–177, 2020.

[4] H. N. Qureshi and A. Imran, "On the tradeoffs between coverage radius, altitude, and beamwidth for practical UAV deployments," *IEEE Transactions on Aerospace and Electronic Systems*, vol. 55, no. 6, pp. 2805–2821, 2019.

[5] D. Alkama, M. A. Ouamri, M. S. Alzaidi, R. N. Shaw, M. Azni *et al.,* "Downlink performance analysis in MIMO UAV-cellular communication with LOS/NLOS propagation under 3D beamforming," *IEEE Access*, vol. 10, pp. 6650–6659, 2022.

[6] X. Cai, C. Zhang, J. Rodríguez-Piñeiro, X. Yin, W. Fan *et al.,* "Interference modeling for low-height air-to-ground channels in live LTE networks," *IEEE Antennas and Wireless Propagation Letters*, vol. 18, no. 10, pp. 2011–2015, 2019.

[7] M. Liu, G. Gui, N. Zhao, J. Sun, H. Gacanin *et al.,* "UAV-aided air-to-ground cooperative nonorthogonal multiple access," *IEEE Internet of Things Journal*, vol. 7, no. 4, pp. 2704–2715, 2020.
[8] Y. Zhou, V. W. S. Wong and R. Schober, "Coverage and rate analysis of millimeter wave NOMA networks with beam misalignment," *IEEE Transactions on Wireless Communications*, vol. 17, no. 12, pp. 8211–8227, 2018.
[9] Ch. Zou, Xi. Li, Xing. Liu and M. Zhang, "3D placement of unmanned aerial vehicles and partially overlapped channel assignment for throughput maximization," *Digital Communications and Networks*, vol. 7, no. 2, pp. 214–222, 2021.
[10] Y. Zhang, Y. Zhou, Z. Ji, K. Lin and Z. He, "A three-dimensional geometry-based stochastic model for air-to-air UAV channels," in *2020 IEEE 92nd Vehicular Technology Conf. (VTC2020-Fall)*, Victoria, BC, Canada, pp. 1–5, 2020.
[11] M. Alzenad and H. Yanikomeroglu, "Coverage and rate analysis for vertical heterogeneous networks (VHet-Nets)," *IEEE Transactions on Wireless Communications*, vol. 18, no. 12, pp. 5643–5657, 2019.
[12] M. Mozaffari, W. Saad, M. Bennis and M. Debbah, "Unmanned aerial vehicle with underlaid device-to-device com-munications: Performance and tradeoffs," *IEEE Transactions on Wireless Communication*, vol. 15, no. 6, pp. 3949–3963, 2016.
[13] E. Turgut and M. C. Gursoy, "Downlink analysis in unmanned aerial vehicle (UAV) assisted cellular networks with clustered users," *IEEE Access*, vol. 6, pp. 36313–36324, 2018.
[14] M. Afshang, C. Saha and H. S. Dhillon, "Nearest-neighbor and contact distance distributions for Matérn cluster process," *IEEE Wireless Communication Letters*, vol. 21, no. 12, pp. 2686–2689, 2017.
[15] W. Yi, Y. Liu, E. Bodanese, A. Nallanathan and G. K. Karagiannidis, "A unified spatial framework for UAV-aided MmWave networks," *IEEE Transactions on Communications*, vol. 67, no. 12, pp. 8801–8817, 2019.
[16] M. M. Azari, F. Rosas, A. Chiumento and S. Pollin, "Coexistence of terrestrial and aerial users in cellular net-works," in *2017 IEEE Globecom Workshops (GC Wkshps)*, pp. 1–6, 2017. https://arxiv.org/abs/1710.03103.
[17] T. Hou, Y. Liu, Z. Song, X. Sun and Y. Chen, "Multiple antenna aided NOMA in UAV networks: A stochastic geometry approach," *IEEE Transactions on Communications*, vol. 67, no. 2, pp. 1031–1044, 2019.
[18] W. Tang, H. Zhang and Y. He, "Tractable modelling and performance analysis of UAV networks with 3D blockage effects," *IEEE Wireless Communications Letters*, vol. 9, no. 12, pp. 2064–2067, 2020.
[19] M. Cheng, J. Wang, Y. Wu, X. Xia, K. Wong *et al.,* "Coverage analysis for millimeter wave cellular networks with imperfect beam alignment," *IEEE Transactions on Vehicular Technology*, vol. 67, no. 9, pp. 8302–8314, 2018.
[20] M. T. Dabiri and S. M. S. Sadough, "Optimal placement of UAV-assisted free-space optical communication systems with DF relaying," *IEEE Communications Letters*, vol. 24, no. 1, pp. 155–158, 2020.
[21] M. A. Ouamri, "Stochastic geometry modeling and analysis of downlink coverage and rate in small cell network," *Telecommunication Systems*, vol. 77, pp. 767–779, 2021.
[22] M. A. Ouamri, M. E. Oteşteanu, A. Isar and M. Azni, "Coverage, handoff and cost optimization for 5G heterogeneous network," *Physical Communication*, vol. 39, no. 5, pp. 101037, 2020.
[23] A. Thornburg and R. W. Heath, "Ergodic capacity in mmWave ad hoc network with imperfect beam alignment," in *MILCOM 2015 - 2015 IEEE Military Communications Conference*, Tampa, FL, USA, pp. 1479–1484, 2015.
[24] M. Afshang and H. S. Dhillon, "Poisson cluster process based analysis of HetNets with correlated user and base station locations," *IEEE Transactions on Wireless Communications*, vol. 17, no. 4, pp. 2417–2431, 2018.
[25] J. G. Andrews, F. Baccelli and R. K. Ganti, "A tractable approach to coverage and rate in cellular networks," *IEEE Transactions on Communication*, vol. 59, no. 11, pp. 3122–3134, 2011.

Appendix A.

The association probability for UAV-UE can be evaluated as

$$\mathcal{A}^k_{UAV} \underset{(a)}{=} \mathbb{P}\left(P_j G_j PL_j,^{k-1} \geq P_i G_i PL_{i'}{}^{-1}\right) \tag{23}$$

$$\mathcal{A}^k_{UAV} \underset{(b)}{=} \mathbb{P}\left(\left(r_j{}^2 + H_z{}^2\right)^{\frac{\alpha^k}{2}} > \frac{P_i G_i A^k}{P_j G_j \varphi^k} r_i{}^{\alpha^k}\right)$$

$$\mathcal{A}^k_{UAV} \underset{(c)}{=} \int_0^\infty 1 - \mathbb{P}(r_j{}^2 > \left(\frac{P_i G_i A^k}{P_j G_j \varphi^k} r_i{}^{\alpha^k}\right)^{\frac{2}{\alpha^k}} - H_z{}^2 \times f_{R_0}(r\,|D,\sigma)$$

where (a) according to the definition of association probability, (b) is due to the path loss model, and (c) follows from conditioning on the closest distance. By applying the null probability of a 2-D Poisson process [24]:

$$\mathcal{A}^k_{UAV} = 1 - \int_0^\infty \exp\left(-2\pi\lambda_{UAV} \int_0^{\sqrt{\omega}} t P^k_{UAV}(t)\right) f_{R_0}(r\,|D,\sigma)\, dr \tag{24}$$

where $\sqrt{\omega} = \left(\frac{P_i G_i A^k}{P_j G_j \varphi^k} r_i{}^{\alpha^k}\right)^{\frac{2}{\alpha^k}} - H_z{}^2$. The association probability for GBS-UE can be evaluated in the same way.

Appendix B.

$$P^k_{C,UA} = P(\gamma_{UAV} > \tau) \tag{25}$$

$$= P\left(\frac{P_{UAV} G_{UAV} h_{UAV} PL^k_{UAV}(r)^{-1}}{I_{UAV'} + \sigma^2} > \tau\right)$$

$$= P\left(h_{UAV} > \frac{\tau PL^k_{UAV}(r)}{m_R m_T P_{UAV}}\left(I_{UAV'} + \sigma^2\right)\right)$$

$$\approx \mathbb{E}_{G_{UAV}}\left[1 - \mathbb{E}_{I_{UAV'}}\left[\left(1 - e^{-\frac{\tau PL^k_{UAV}(r)}{m_R m_T P_{UAV}}\left(I_{UAV'} + \sigma^2\right)}\right)^{N_k}\right]\right] \tag{26}$$

$$= \mathbb{E}_{G_{UAV}}\left[\sum_{n=1}^{N_k} (-1)^{n+1} \binom{N_k}{n} \mathbb{E}_{I_{UAV}}\left[e^{-\mu\left(I_{UAV} + \sigma^2\right)}\right]\right] \tag{27}$$

$$P^k_{C,UAV} = \mathbb{E}_{G_{UAV}}\left[\sum_{n=1}^{N_k} (-1)^{n+1} \binom{N_k}{n} e^{-\mu\sigma^2} \mathcal{L}_{I_{I_{UAV'}}}(\mu)\right] \tag{28}$$

where $\mathcal{L}_{I_{I_{UAV'}}}(\mu)$ is the Laplace transform which is the relevant intermediate step of the coverage analysis. Eq. (26) follows the Binomial theorem and the assumption that N_k is an integer [25]. Then, Eq. (27) follows from the independence between the interference $\mu = \frac{\tau \varphi^k (r^2 + H_z{}^2)^{\frac{\alpha^k}{2}}}{P_{UAV} m_R m_T}$. However, $\mathcal{L}_{I_{I_{UAV'}}}(\mu)$ can be compute a

$$\mathcal{L}_{I_{I_{UAV'}}}(\mu) = \mathbb{E}\left[e^{-\mu I_{UAV'}}\right]$$

$$= \mathbb{E}\left[\exp\left(-\mu \sum_{UAV' \neq UAV} P_{UAV'} G_{UAV'} h_{UAV'} PL^{k}_{UAV'}(r)\right)\right]$$

$$-2\pi\lambda_{UAV}\mathbb{E}_{m_R m_T}\exp\left(\left[\left(\int_{x}^{\infty} \mathbb{E}_{h_{UAV}}\left[e^{-\mu P_{UAV'} G_{UAV'} h_U PL^{k}_{UAV'}(r)}\right]\right) rP^{k}_{UAV'}(r)\, dr\right]\right)$$

$$= exp\left(\left[-2\pi\lambda_{UAV}\mathbb{E}_{m_R m_T}\left(\int_{x}^{\infty} 1 - \left(\frac{1}{1+\frac{\mu P_{UAV'} G_{UAV'} PL^{k}_{UAV'}(r)}{N_k}}\right) rP^{k}_{UAV'}(r)\, dr\right]\right)$$

Proof of the Laplace transform $\mathcal{L}_{I_{GBS'}}(\mu)$ and $\mathcal{L}_{I_{I_{UAV}}}(\mu)$ follows the same steps as $\mathcal{L}_{I_{UAV'}}(\mu)$.

$$\mathcal{L}_{I_{GBS'}}(q) = \exp\left(-2\pi\lambda_{GBS} \times \mathbb{E}_{m_R m_T}\left[\left(\int_{x}^{\infty} 1 - \left(\frac{1}{1+\frac{qP_{GBS'} G_{GBS'} PL^{k}_{GBS'}(r)}{N_k}}\right)^{N_k}\right)\right]\right) \tag{29}$$
$$rP^{k}_{GBS'}(r)\, dr$$

$$\mathcal{L}_{I_{I_{UAV}}}(\mu) = \exp\left(-2\pi\lambda_{UAV} \times \mathbb{E}_{m_R m_T}\left[\left(\int_{x}^{\infty} 1 - \left(\frac{1}{1+\frac{\mu P_{UAV} G_{UAV} PL^{k}_{UAV}(r)}{N_k}}\right)^{N_k}\right)\right]\right) \tag{30}$$
$$rP^{k}_{UAV}(r)\, dr$$